PAPER

Photothermally-driven thermo-oxidative degradation of low density polyethylene: heterogeneous heating plus a complex reaction leads to homogeneous chemistry

IOP Publishing Nanotechnology
Nanotechnology 30 (2019) 475706 (14pp) https://doi.org/10.1088/1361-6528/ab3bc0

Photothermally-driven thermo-oxidative degradation of low density polyethylene: heterogeneous heating plus a complex reaction leads to homogeneous chemistry

Gabriel Firestone[1], **Honglu Huang**[2], **Jason R Bochinski**[1,3] and **Laura I Clarke**[1,3]

[1] Department of Physics, North Carolina State University, Raleigh, NC 27695, United States of America
[2] Fiber and Polymer Science, North Carolina State University, Raleigh, NC 27606, United States of America

E-mail: jrbochin@ncsu.edu and laura_clarke@ncsu.edu

Received 5 June 2019, revised 28 July 2019
Accepted for publication 15 August 2019
Published 9 September 2019

Abstract

Photothermal heating from embedded nanoparticles, a process whereby visible light is converted into heat resulting in a high temperature in each particle's immediate vicinity, was utilized to degrade low density polyethylene (LDPE) via thermo-oxidation. The spatially-varying steady-state photothermal temperature field is a potential mechanism by which ambient light (e.g. sunlight) could be used to drive chemical reactions within solid materials and may result in a non-uniform pattern of products, an advantage or disadvantage depending on application. Novel approaches to control polymer degradation are of interest because of the goal of remediating plastic waste, including autonomous means to minimize its effect when unconfined in the environment. For thermoplastic auto-oxidation, heterogeneous degradation would likely enhance deleterious micro-fragmentation however, the multi-step, multi-site nature of the reaction mitigated the temperature non-uniformity. A photothermally-heated LDPE nanocomposite with silver nanoparticle and cobalt-stearate additives showed degradation, characterized by ultraviolet–visible and Fourier-transform infrared absorption spectroscopy, electron microscopy, and mechanical testing, nearly identical to that resulting from uniform conventional treatment at the same average temperature.

Supplementary material for this article is available online

Keywords: autonomous chemistry, local chemistry, nanocomposites, photothermal heating, degradation

(Some figures may appear in colour only in the online journal)

1. Introduction

The concept of facilitating high-societal-impact chemical reactions via utilization of available solar illumination [1] is compelling due to its practicality, association with green chemistry principles, and connection to natural chemical processes such as photosynthesis. For instance, addition of a 'sensitizer' to a material in order to significantly enhance the absorption of light provides a mechanism to collect energy which can drive an internal chemical reaction. Photothermal processes, like those associated with metal nanoparticles (or other less expensive nano-objects [2, 3]) that interact with light and convert it into local heat [4–9] , are natural choices for exploration of this paradigm. When considering useful

[3] Authors to whom any correspondence should be addressed.

chemistry that would ideally proceed spontaneously under exposure to sunlight, strategies for passive environmental plastic remediation represent a worthy goal. The harmful presence of commodity plastics in the environment has been well-documented [10–13] and includes damage to marine and terrestrial animals [14–17], increased strain on water treatment facilities [18, 19], and concentration of hydrophobic toxins [20–23].

While oxidative degradation of thermoplastics in principle can be implemented either by exposure to ultraviolet (UV) light or heat, in practice the small UV absorption cross-section limits photo-oxidation under typical light sources and the thermal oxidation rate is slow at room temperature, requiring a time scale of years [24–26] for any significant effect. Thus an intentional temperature increase is needed if thermo-oxidation is the desired degradation pathway. We note that UV activated photodegradation of polyethylene can be enhanced through the addition of certain nanofillers [27–31]. Both of these degradation processes rely on chemical defects (such as non-saturated bonds) within the polymer to initiate so-called autoxidation [32]. Furthermore, the minute fraction of degradation that does occur under ambient conditions significantly impacts mechanical strength, detrimentally leading to micro-fragmentation where chemically intact (and thus strongly hydrophobic) materials break into small pieces [33–35]. This phenomenon is particularly environmentally damaging for material in the oceans as hydrophobic toxins (such as pesticides) adhere to plastic particulates, which are small enough to be easily ingested by marine animals [16, 36, 37]. Once in such a micro-fragmented state, realistic environmental remediation is virtually impossible [38]. Thus, any strategy to enhance degradation for polymeric objects unconfined in the environment would ideally significantly enhance degradation, be autonomous, and not increase micro-fragmentation of the material.

Nanoparticle-based photothermal heating processes are a natural choice to explore when considering autonomous energy collection. The photothermal mechanism is characterized by high efficiency (i.e. an almost perfect conversion of the energy of each absorbed photon to heat) [38–40] and internal temperature increases on the order of 100 °C can be accomplished in ambient conditions under moderate light intensity with relatively dilute particle concentrations (e.g. hundredths of a weight percent) [41–45]. Such temperatures attained with conventional means are often utilized to facilitate thermal oxidation of polyethylene in accelerated aging studies [46–48]: here, optimally the material would heat itself to these levels in the environment without any human intervention. For metal particles, the localized surface plasmon resonance (SPR) that determines the absorption spectrum is influenced by the composition, size, and shape of the particles, as well as the dielectric environment (i.e. the surrounding polymer). For instance, easily fabricated, relatively inexpensive, silver nanoparticles with a slight polydispersity of sizes (such as those used in this work) incorporated into a polymer matrix generally absorb wavelengths in the range 326–504 nm, centered on the blue band and encompassing about half of the visible light spectrum, thus providing efficient energy collection of sunlight. While silver nanoparticles represent a convenient, efficient choice of photothermal agent for the work presented here, other metal nanoparticles (i.e. gold, copper, or aluminum) or nano-objects (e.g. carbon nanotubes) are also potential candidates [49, 50]. We note that blue light (400–430 nm) is minimized in most modern indoor lighting due to the human eye's inefficiency at shorter wavelengths and customer preference for 'warmer' (i.e. more red and yellow hues) light [51, 52]. This selectivity might provide specificity for primarily driving degradation only when the material is intentionally exposed to certain light sources and not during normal use.

A distinctive characteristic of photothermal heating at low nanoparticle concentration is a strongly inhomogeneous steady state temperature distribution [4, 41, 43, 45]. Heat is continuously generated by each individual nanoscopic particle. For a completely isolated particle in a thermally insulating medium, the steady state temperature falls off as $\frac{\sim 1}{r}$ moving away from the particle and the temperature pattern will be similar for low concentration cases. For instance, for inter-particle spacing $>10\times$ the particle dimension, temperature differences between material near and far from a particle can exceed 50 °C. Heterogeneous temperatures might create uneven spatial degradation throughout the material and thereby mechanical defect formation, leading to deleterious loss of structural integrity. However, oxidative degradation reactions are a multi-step process requiring not only heat but also the presence of oxygen, chemical defects, and radicals formed by previous bond-breaking [53] which may minimize the position-specific effect of the heterogeneous heating (vide infra). Polyethylene oxidation within a solid material is often limited by diffusion of oxygen into the interior. Furthermore, if a pro-oxidant agent such as a metal complex [54] (e.g. cobalt stearate) is used to catalyze the reaction, then radical formation will be more efficient near pro-oxidant sites. Thus, while the oxygen rich regions extend from the exterior of the sample inward, the pro-oxidant sites, defects, and hot regions from photothermal heating are randomly-distributed. Consequently, degrading reactions will optimally occur only where all of these elements overlap, thus potentially mitigating any negative effects of the spatially inhomogeneous temperature profile within the sample.

In this work, use of photothermal heating to drive oxidative degradation of low-density polyethylene (with cobalt stearate as a pro-oxidative agent to enable tractable degradation times) is demonstrated. The light intensity used was approximately 20 times that of the Sun in the relevant spectral output range. We utilize measurement spectroscopy from UV to infrared wavelengths to quantify the resultant reactions, and independently track mechanical properties and sample morphology. Degradation via photothermal heating is identical to that achieved by conventional treatment at the same average temperature (60 °C), which indicates that thermo-oxidative degradation could be autonomously driven by application of light to result in accelerated aging without requiring any overt intervention. More broadly, these proof-of-principle results indicate that photothermal heating is

capable of driving chemical reactions homogeneously and autonomously within a solid material if a suitable reaction is selected.

2. Experimental

2.1. Materials

Low-density polyethylene homopolymer (LDPE) (Petrothene NA940000, LyondellBasell Industries) (Melt Flow Index (MFI) 0.25 g/10 min, Density 0.918 g cm^{-3}, Vicat softening temperature 90 °C) and Cobalt(II) stearate pellets (Santa Cruz Biotechnology, Inc) were processed into fine powders before use. Aqueous silver nitrate (ASTM reagent grade, Ricca Chemical), dioctyl sulfosuccinate sodium salt (AOT) (Purum grade, Sigma Aldrich), Lumogen F Orange 240 (Lumogen Orange) (BASF SE), toluene and acetone (ACS reagents grade, Fisher Chemical) were used as received.

2.2. Silver nanoparticle synthesis

Silver nanoparticles (AgNPs) were synthesized by a reverse micellar reduction of silver nitrate [55–57]. Under intense stirring 200 μl of 0.1 M aq. $AgNO_3$ was added to 20 ml of 0.25 M AOT in toluene in a glass vessel. The vessel was sealed and stirring continued for an hour as the solution first turned clear, indicating successful micelle formation, then light yellow as nanoparticle seeds formed. The sealed vessel was placed in a 100 °C oven for two hours to accelerate nanoparticle growth by enhanced silver ion reduction. The resulting nanoparticle emulsion was allowed to cool, then centrifuged for 10 minutes at 16.1 kRCF and supernatant replaced with fresh toluene to remove excess AOT and water. The process was repeated without redilution to produce a ~10 nM [58, 59] concentrated solution of AOT-stabilized AgNPs in toluene.

AgNPs were characterized by extinction spectroscopy (UV–vis)(Cary Scan 50), and exhibited a strong plasmonic absorption peak centered at 429 nm with a full-width-at-half-maximum (FWHM) of 107 nm as shown in figure 1. The observed SPR peak wavelength matches that of a Mie theory prediction for a monodisperse solution of 25 nm diameter AgNP, which would have a FWHM of 35 nm. The larger experimentally-observed peak width indicates some polydispersity of particle sizes. We note as a practical consideration, that the wider absorption range of polydisperse AgNPs actually better matches the output of broad spectrum energy sources, such as sunlight. The upper inset shows a transmission electron spectroscopy (TEM) image of the nanoparticles. Analysis of multiple higher magnification images enable measurement of particle size using ImageJ software, resulting in 17 ± 10 nm, consistent with the spectroscopy results. The lower inset depicts a histogram of the measured AgNPs diameter values.

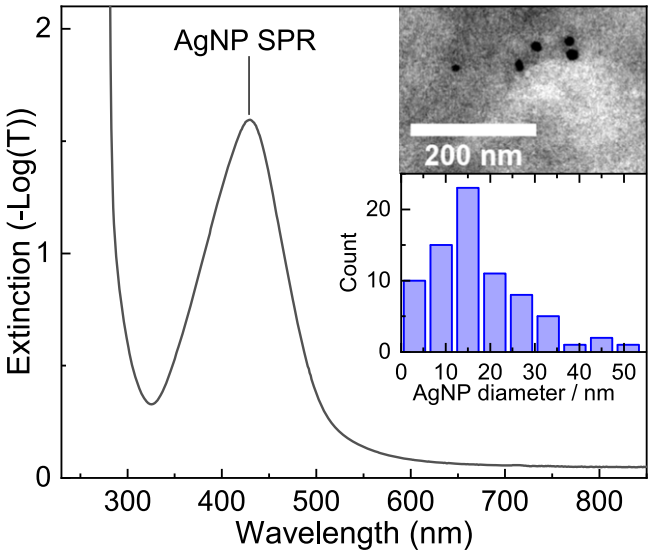

Figure 1. Extinction spectrum of AgNPs, diluted to 0.5 nM in toluene. Inset: top—TEM image of a dropcast sample of the same solution. Bottom—a histogram of AgNPs diameter values ($N = 76$) from a series of TEM images.

Table 1. LDPE Formulations.

Name	AgNP (wt%)	Cobalt stearate (wt%)	Lumogen orange (wt%)
PE-neat	—	—	—
PE-AgNP	0.002	—	—
PE-Co	—	1.0	—
PE-AgNP-Co	0.002	1.0	—
PE-AgNP-Lum	0.002	—	0.0005

2.3. Polymer nanocomposite film preparation

LDPE pellets were cryo-ground in liquid nitrogen (Spex 6870 Freezer/Mill) to reduce the particle size and ease incorporation of additives. Cobalt(II) stearate pellets were ground into a fine powder by mortar and pestle. Master batches of LDPE containing 0.0005 wt% Lumogen F Orange 240 (Lumogen) and/or 1 nM AgNPs were prepared by wetting LDPE powder with either AgNPs in toluene or Lumogen in acetone, then mixing until the solvent fully evaporated. Powdered cobalt(II) stearate was incorporated into LDPE powder at a concentration of 1 wt% immediately prior to film creation.

Film samples were prepared by melt-pressing: three grams of master batch powder and several 0.5 mm thick spacers were placed between sheets of non-stick aluminum foil (Kroger Corporation) and subjected to five metric tons force (50 kN) for 30 seconds in a hydraulic press (Carver 3851–0) with heated platens at 150 °C. The newly formed film was quench cooled, removed from the foil, cut into pieces, and stacked on fresh foil to be re-pressed. This process was twice repeated to aid additive dispersion within the film. During the final melt-press, the force was applied for 5 min to facilitate polymer equilibration. The formulation and naming scheme for each film type is given in table 1. The resulting

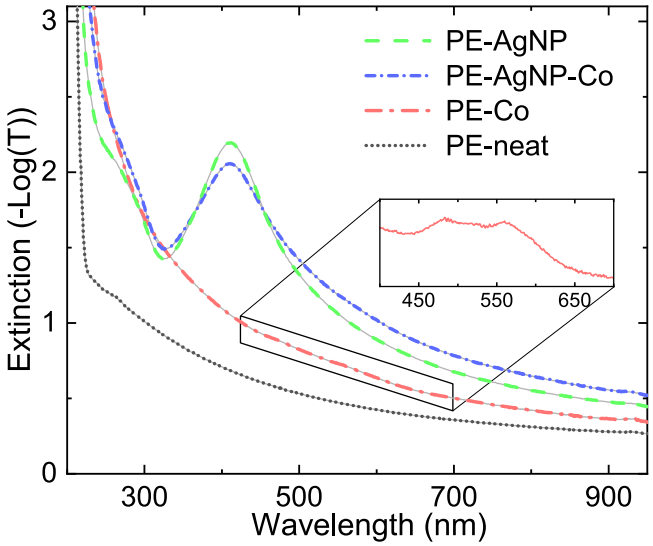

Figure 2. Extinction spectra of neat and composite LDPE (PE) film samples containing cobalt stearate (Co) and silver nanoparticles (AgNP). The large peak at 410 nm is due to the SPR of AgNPs, and the broad absorption from 450–600 nm is associated with cobalt(II). Inset shows the cobalt(II) region after subtraction of a matched PE-neat spectrum.

films were measured to be 0.28 ± 0.05 mm thick by digital calipers.

2.4. Nanocomposite film characterization

To confirm dispersion of both AgNPs and Cobalt species within the LDPE matrix extinction spectroscopy and electron microscopy were utilized. In the spectra shown in figure 2, the distinct AgNPs SPR absorption peak (at 429 nm in solution) is present in both PE-AgNP and PE-AgNP-Co samples. The peak location reflects both the average particle size and the surrounding dielectric environment (which is similar for PE (n = 1.45–1.55) and toluene (n = 1.52)). The similarity of the extinction peak position in solution and solid indicates that within the existing polydispersity, the average particle size did not significantly increase. In a corresponding fashion, the width of the peak reflects the distribution of particle sizes and nearly identical widths for solid samples of PE-AgNP and PE-AgNP-Co (96 and 95 nm, respectively) and AgNP in solution (107 nm) were observed, indicating that no significant aggregation is present when placed in the solid. TEM images confirm the presence of AgNPs (dark spheres) and size analysis (N = 76) results in an average diameter 17 ± 10 nm, in agreement with the extinction spectra. Dispersion can be also quantified by counting the cases where the nearest neighbor spacing between particles exceeds two times their radius, the minimum distance below which undesirable particle–particle interactions significantly impact efficiency [60, 61]. 88% of 144 measured nearest neighbor distances exceeded this measure.

The AgNPs concentration predicted from the Beer–Lambert law and the observed peak size in the extinction spectrum was 1 nM, indicating that a significant fraction of AgNPs survived the film creation and were independently plasmonically-active. The particle concentration estimated via TEM is consistent with this value. The average concentration of nanoparticles within the solid LDPE samples can be roughly estimated by dividing the total number of particles counted across 73 images by the total imaged volume, giving a result of 5 nM . This value likely represents an overestimate due to observed AgNP clustering (several closely-spaced but not aggregated particles in one area) and oversampling of regions with particles by TEM, which is consistent with its value as 5x that from the macroscopic optical measurement.

In the extinction spectra (figure 2), the broad absorption from 450–600 nm in PE-Co and PE-AgNP-Co films indicates the presence of cobalt(II) ions in the samples [62, 63]. Unlike AgNPs, the successful dispersion of cobalt ions into the LDPE matrix is more difficult to directly confirm via TEM as such images can only identify the presence of cobalt aggregates. Figure 10 (images b, c, e, f, h, i) contain cobalt. No aggregates were observed in images of LDPE that contained only cobalt additives, indirectly demonstrating adequate dispersion. The surrounding LDPE matrix (gray areas) appears largely featureless in as-made samples, with subtle variation in shade due to changes in cross-section thickness from the micro-toming process or subsequent buckling. The matrix shows no defects in the vicinity of AgNPs indicating good bonding between the nanoparticles and the polymer.

2.5. Photothermal and conventional thermal oxidation

Photothermal-oxidative tests (PT aged) utilized a lab-constructed blue light source wherein film samples were illuminated from below by an array of royal blue LEDs (443 nm emission peak with a 15 nm FWHM) at an intensity of 0.27 ± 0.06 W cm^{-2} for 120 h. Ambient temperature in the irradiation environment was 36 °C. For comparison, thermo-oxidative tests (oven aged) on nanocomposite film samples were also performed in a conventional, gravity convection oven at 55 °C–60 °C for 120 h.

2.6. Evaluation of degradation

Oxidative degradation of LDPE was measured using extinction spectroscopy (UV–vis), Fourier transform infrared absorption spectroscopy (FTIR), mechanical tensile properties, and electron microscopy to reveal surface (SEM) or internal (TEM) sample morphology.

Tensile properties were evaluated using a universal Testing Machine (Instron 5944) with 50 N load cell. The modulus, tensile strength at break and elongation at break were measured at a testing speed of 40 mm min^{-1}. Specimens had a gauge length of 48 and 10 mm width. Each sample condition was replicated with at least 10 specimens. An average value and standard deviation are reported. FTIR absorption spectra were recorded on an integrated bench (Thermo Fisher iS50) in attenuated total reflectance mode using a diamond crystal. 64 scans of 4 cm^{-1} resolution were averaged per spectrum and converted to absorbance via built-in software, with resulting repeatability of 0.3% of full scale. The diamond crystal reflector resulted in minor noise in the

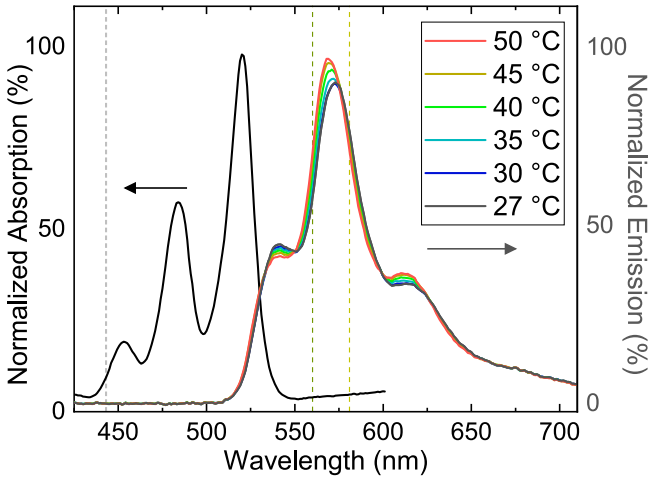

Figure 3. Absorption spectrum (left) of Lumogen Orange F 240 in LDPE. Emission spectra (right) at increasing temperatures exhibit distinct changes that are utilized for temperature measurement. Dashed lines indicate wavelengths used for excitation and those used determine intensity ratios for thermometry.

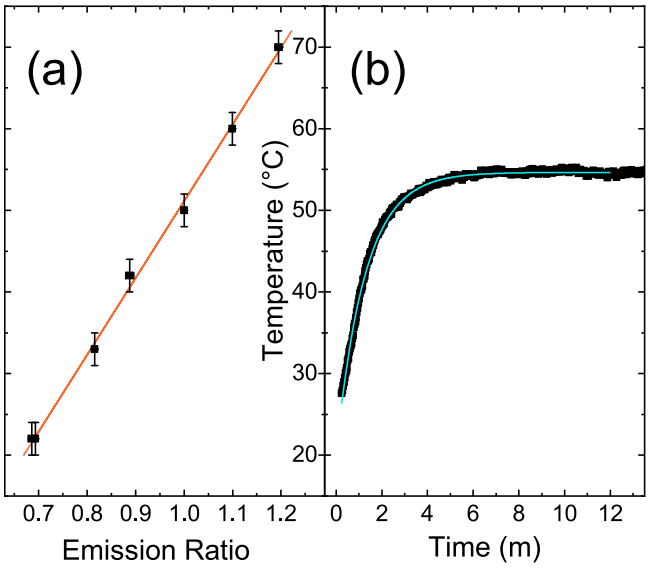

Figure 4. (a) Black square data points plot the intensity ratio of Lumogen fluorescence at six sample temperatures, with linear fit (orange line). (b) Measured temperature increase in PE-AgNP-Lum due to photothermal heating after the excitation light is applied at time $t = 0$ s, with a single exponential fit (blue line).

region from 2300–1900 cm^{-1}, which is not a region of interest. UV–vis extinction spectra with 1 nm resolution and 0.25 s integration time was used to monitor growth of UV-absorbing oxidation products as well as the presence of additives (AgNPs, cobalt stearate, and Lumogen orange). Surface morphological images were collected on a variable pressure SEM (Hitachi S3200N) at 2500x magnification (20 kV). Specimens were sputter coated with ~30 nm of gold prior to imaging to reduced charging effects. Internal morphological images were collected on specimens that had been ultra-microtomed to ~100 nm thickness, then examined via TEM (JEOL 2000FX) at 200 kV electron energy.

2.7. Non-contact temperature measurement

As reported previously [8, 9, 43, 45, 64–68], perylene molecules can be incorporated into a polymer matrix as a minute additive and utilized for fluorescence thermometry to monitor average sample temperature. In this work, the perylene-derivative dye Lumogen F Orange 240 was employed, which shares key properties with its progenitor: namely, good photostability, ease of incorporation into non-polar media, and a multi-peaked fluorescence spectrum. The absorption and emission spectral features of Lumogen Orange are red-shifted by ~100 nm as compared to perylene, which results in some overlap between the absorption bands of Lumogen Orange and the AgNPs. Consequently, the same light source (see section 2.4) can be utilized to excite both the plasmonic nanoparticles and the fluorescent dye. Under such illumination, the samples warmed to a steady-state temperature in approximately 5 min, which enabled accurate determination of the value before significant photobleaching occurred. The high intensity light (0.27 W cm^{-2}) used to drive the nano-heaters however did increase the photobleaching rate of the dye, with a $1/e$ time constant measured at 2 h at room temperature. Lumogen fluorescence was collected by a 1 inch diameter lens, spectrally-filtered to reject scattered excitation light, then coupled through a fiber optic cable into a spectrometer (Ocean Optics Flame) with 25 μm slits having 1.4 nm overall resolution using 0.1 s integration time.

Figure 3 shows the spectrally-resolved absorption and emission scans of Lumogen F Orange 240 incorporated in LDPE. The peaks correspond to transitions between the various vibrational levels of the first excited electronic state of the Lumogen molecule and the ground state. Emission spectra are shown for six different temperatures from 27 °C–50 °C. The changes in the spectra with temperature can be analyzed to deduce temperature. Here, a ratiometric approach was utilized by computing all possible intensity ratios (the fluorescence intensity at wavelength x divided by the fluorescence intensity at wavelength y plotted versus temperature) and then selecting the combination with the most linear response over the temperature range of interest. Such a method is robust to variation in illumination intensity and photobleaching, and relatively simple to calculate. Figure 4(a) shows the optimal, selected intensity ratio (where $x = 560$ nm and $y = 581$ nm), demonstrating its linearity with temperature. 560 nm is on the blue side of the central peak while 581 nm lies on the red side.

To determine the temperature of photothermally heated samples, specimens containing AgNPs and Lumogen Orange (PE-AgNP-Lum) were irradiated by the LED light source and monitored as they came to steady-state (figure 4(b)). A steady-state temperature of 55 ± 1 °C was measured for all times after 5 min under light intensity of 0.27 W cm^{-2}. Internal temperatures determined via this approach are the result of an ensemble measurement of fluorescence from molecules distributed throughout the entire specimen and thus, represent an average temperature value away from the intensely heated (but very small) regions surrounding each particle. As discussed below and in the introduction, the distributed nature of the multi-step reactions that lead to

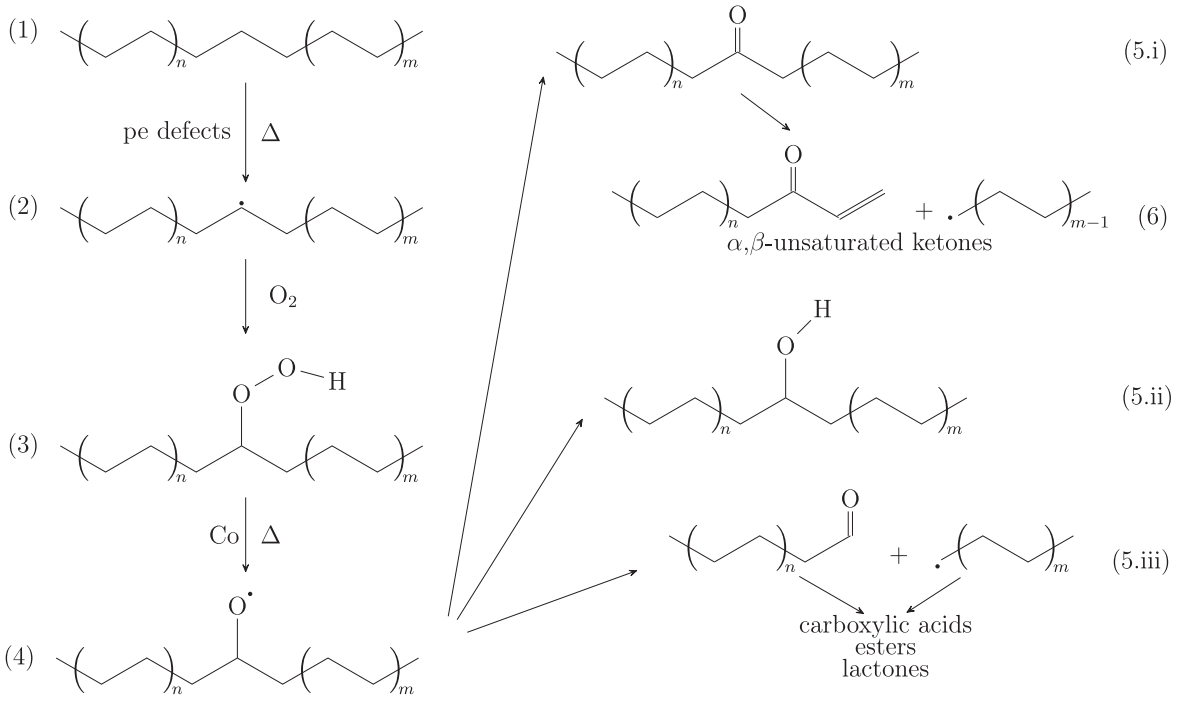

Scheme 1. A simplified scheme summarizing the thermo-oxidative degradation of polyethylene and the relevant degradation products. Thermal degradation is initiated (1) when a hydrogen atom is abstracted from the chain by heat and nearby defects creating a polymer free radical (2). The radical reacts with oxygen to incorporate hydroperoxides onto the chain (3). The pro-oxidant cobalt ions catalyze the splitting of these hydroperoxides into alkoxy radicals (4). These alkoxy radicals enable various reactions which produce carbonyl groups (5.i), hydroxides (5.ii), and backbone modified groups (5.iii) monitored via FTIR, as well as conjugated ketones monitored by UV–vis absorption spectroscopy (6).

oxidative degradation in PE means that the degradation process is unlikely to be significantly affected by the hot-spots around each particle, and thus the average temperature should be the most appropriate comparison with conventionally (i.e. oven-heated) treated samples.

3. Results and discussion

3.1. Characterization of chemical degradation

The chemical changes characteristic of thermal oxidation of polyethylene can be observed using FTIR and UV–visible absorption spectroscopy. The average temperature within the photothermally-heated PE-AgNP-Co samples while illuminated by the blue light source was 55 ± 1 °C and thus results were compared to samples conventionally heated at 55 °C–60 °C for the same time period (up to 120 h). Sample degradation as quantified by these measures proceeded identically when heating either photothermally or conventionally; consequently the figures shown below only detail results from photothermal treatment. Prior work on thermo-oxidation [25] has established a reaction pathway that is summarized in scheme 1.

Figure 5 summarizes FTIR spectra of PE-AgNP-Co samples as a function of photothermal heating time. The peaks at 2915, 2850, 1470, and 720 cm^{-1}, which correspond to the stretching and bending modes of the C–H bonds of the polyethylene backbone, showed no change. With increasing degradation time, infrared absorption increased in several areas: a broad region from 3500 to 2500 cm^{-1}, a series of smaller peaks from 1400 to 700 cm^{-1}, and a complex peak near 1700 cm^{-1}. Most notable is the complex carbonyl peak at 1700 cm^{-1} (figure 5 inset), which consists of multiple nearby peaks belonging to various carbonyl containing compounds. The growing presence of carbonyl groups is a useful indicator of degradation in polyethylene. The addition of oxygen into the polyethylene chain as carbonyl groups is a key step in oxidative degradation, and carbonyl groups decrease the overall stability by enabling further reactions that modify and ultimately break the polymer chain (see scheme 1).

Decomposing the carbonyl peak into constituents, the largest sub-peak is centered at 1713 cm^{-1}, which is indicative of the presence of carboxylic acids in the sample. This can be confirmed by the simultaneous presence of the broad structure from 3500 to 2500 cm^{-1}, corresponding to an O–H stretch with hydrogen bonding; a small peak at 944 cm^{-1} for O–H wag/bend; and a peak in the 1320–1210 cm^{-1} range for C–O stretch. The next largest sub-peak is occurs at 1735 cm^{-1}, indicating the presence of ester groups in the sample. Ester presence can be confirmed by the coexistence of peaks at 1180 cm^{-1} and 1040 cm^{-1}, corresponding to the acyl and alkyl C–O stretch, respectively. On the high wavenumber shoulder, a peak at 1780 cm^{-1} indicates the presence of small ring lactones, which is difficult to confirm with secondary peaks, and on the low wavenumber shoulder, the broad region indicates the presence of carbonyl groups with nearby unsaturations, including conjugated ketones.

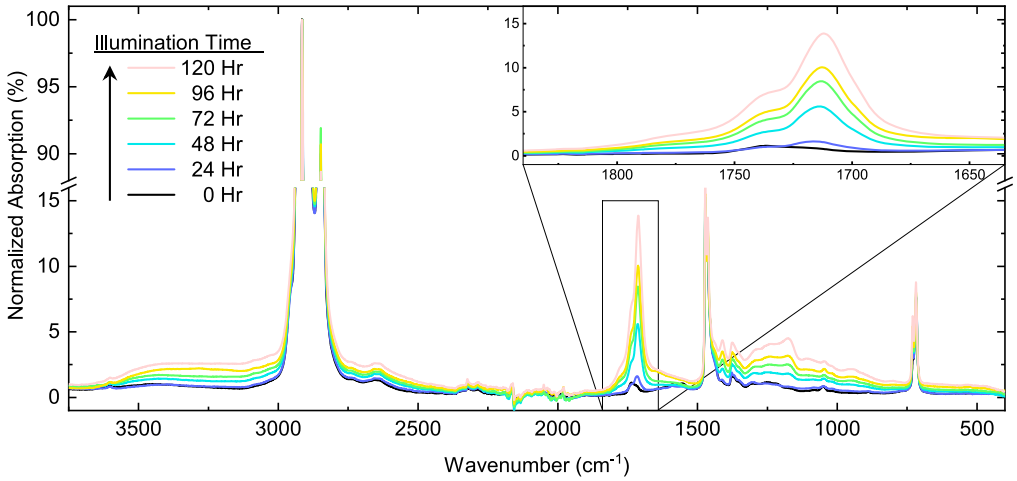

Figure 5. Infrared spectra of PE-AgNP-Co as a function of illumination time. Inset shows the individual peaks comprising the carbonyl peak region.

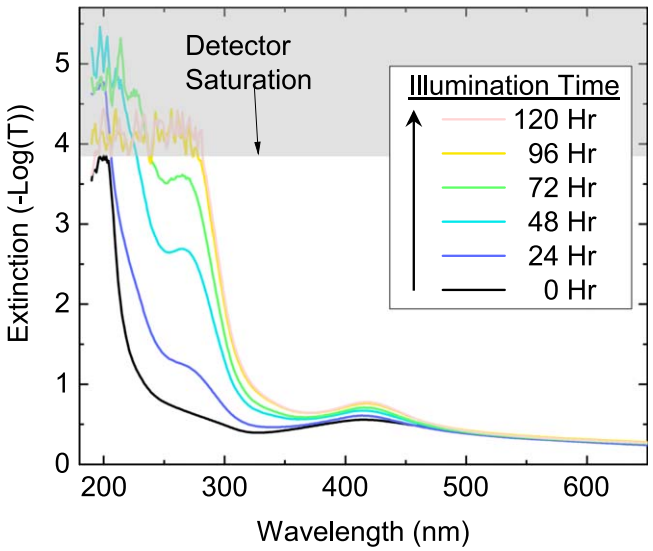

Figure 6. Sequential UV–vis spectra of PE-AgNP-Co reveal conjugated ketone formation due to oxidative degradation as the peak at 275 nm increases as a function of illumination time. In the high absorption region (i.e. values above 4), the detector cannot quantify the remaining (less than 0.01% of the incident light level) intensity. The peak centered around 425 nm is due to the presence of AgNPs (see figures 1 and 2): Note that the slight redshift of the AgNPs peak position with illumination time is likely due to formation of a thin layer of silver oxide upon long term exposure to elevated temperature [69]; see also figures S.3 and S.7 in supplementary information available online at stacks.iop.org/NANO/30/475706/mmedia.

Conjugated ketones, although only weakly displayed in FTIR spectra, have a very strong absorption in the UV–visible spectral range, which has previously been utilized to track PE degradation [25]. The nearby α, β-unsaturation shifts the strongly absorbing $\pi \rightarrow \pi^*$ transition of the carbonyl group from below 200 to 275 nm. Figure 6 shows the effect of photothermal heating on the UV absorption of PE-AgNP-Co samples. With increasing degradation time, a peak appears in the spectrum at 275 nm, which grows and eventually exceeds the measurement capabilities of the detector (see figure 6 caption). In combination with the observation of conjugated ketones signals within FTIR spectra and previous literature precedent [25], we associate the peak at 275 nm with the increasing presence of α, β-unsaturated ketones in the sample.

The four carbonyl types identified above can be tied to the thermo-oxidative degradation reaction pathway as follows (see scheme 1). Lactones and conjugated ketones remove a saturating hydrogen resulting in tertiary carbons and double bonds in the carbon backbone with increased susceptibility to further degradation. Previous work has argued that autoxidation in PE is driven by unsaturated defects [32]. Esters result from insertion of an oxygen molecule into the backbone, modifying the innate hydrophobicity of the chain. Carboxylic acids are associated with chain ends since the carbonyl carbon can only bond to one alkyl chain. It is extremely unlikely that only pre-existing chain-end groups are replaced with carboxylic acid: as a result, the presence of carboxylic acids corresponds to chain breakage. The height of the carboxylic acid carbonyl peak at 1713 cm^{-1} is thus proportional to the concentration of chain breaks. The relative ratios of the four carbonyl peaks change little as a function of exposure time or method, and as such each could be used as a proxy for degradation.

3.2. Comparing chemical degradation as a function of heating modality

Figure 7 plots the growth of the 1713 cm^{-1} carboxylic acid FTIR peak as well as the 275 nm α, β-unsaturated ketone UV–vis peak for all sample types and heating conditions. For samples conventionally heated, those containing cobalt (PE-Co, red squares and PE-AgNP-Co, blue squares) showed an increase in both signals proportional to exposure time, while cobalt-free samples (PE-neat, black squares and PE-AgNP, green squares) revealed no change. These results demonstrate the expected catalytic effect of cobalt as a pro-oxidant which increases the rate of degradation. Previous work [70] indicated that cobalt

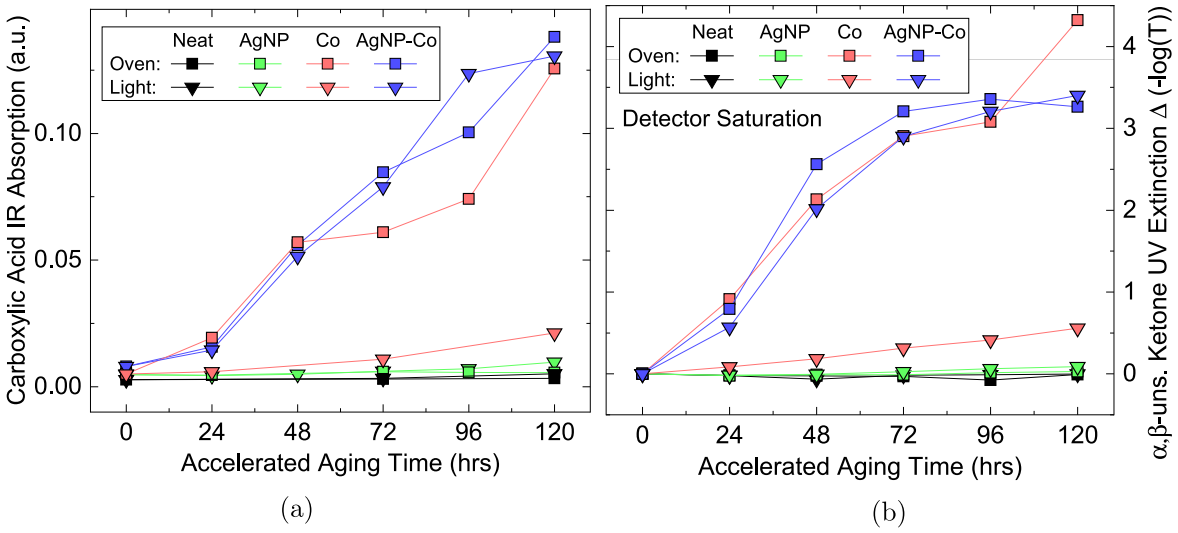

Figure 7. Amplitude of the carboxylic acid FTIR peak (a) and ketone UV–vis peak (b) as a function of illumination time for neat LDPE (black) and that containing silver nanoparticles (green), cobalt stearate (red), and both silver nanoparticles and cobalt stearate (blue). The 'oven' condition refers to conventional heating at 55 °C–60 °C. The 'light' condition refers to photothermal heating, resulting in an average internal sample temperature of 55 °C.

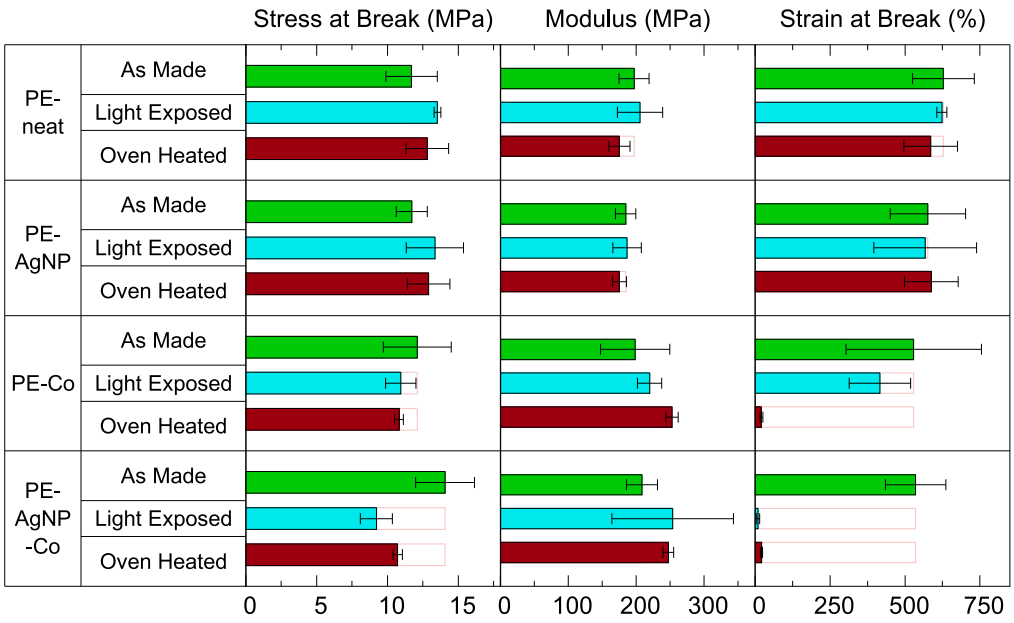

Figure 8. Comparison of the tensile properties of LDPE samples as-made and after 120 h of accelerated aging through conventional or photothermal heating mechanisms. 'As Made' indicates unaged samples (green); 'Light Exposed' indicates under illumination at 0.27 W cm^{-2} from the lab-made source (blue); 'Oven Heated' indicates conventionally heated to 55 °C–60 °C (red).

interacts with step 3 in the reaction chain shown in scheme 1, enhancing the decomposition of alkyl hydroperoxides to enable formation of alkyoxy radicals. Thus the presence of cobalt enables observation of the thermally-driven chemical reaction on a shorter time scale. Samples with silver nanoparticles (PE-AgNP-Co, blue squares) degraded at a similar rate as those without (PE-Co, red squares) indicating that the presence of silver nanoparticles has neither a deleterious nor protective effect.

The presence of cobalt was also needed when heating via the photothermal process. Cobalt-free PE-AgNP samples (green triangles) absorbed light, underwent photothermal conversion, and warmed, resulting in an internal average temperature of 55 °C ± 1 °C (as determined by fluorescence thermometry), however even at this elevated temperature (a similar case to the conventional heating of PE-AgNP, green squares), no significant deterioration-driven peaks were observed. For samples lacking both cobalt and AgNP (PE-neat, black triangles), illumination resulted in no change, as expected. Overall these results indicate that the only chemical reactions observable on this time scale are cobalt-catalyzed thermo-oxidation.

Examining the effect of illumination on cobalt-containing samples, figure 7 indicates that PE-AgNP-Co samples (blue triangles) which contained silver nanoparticles showed a

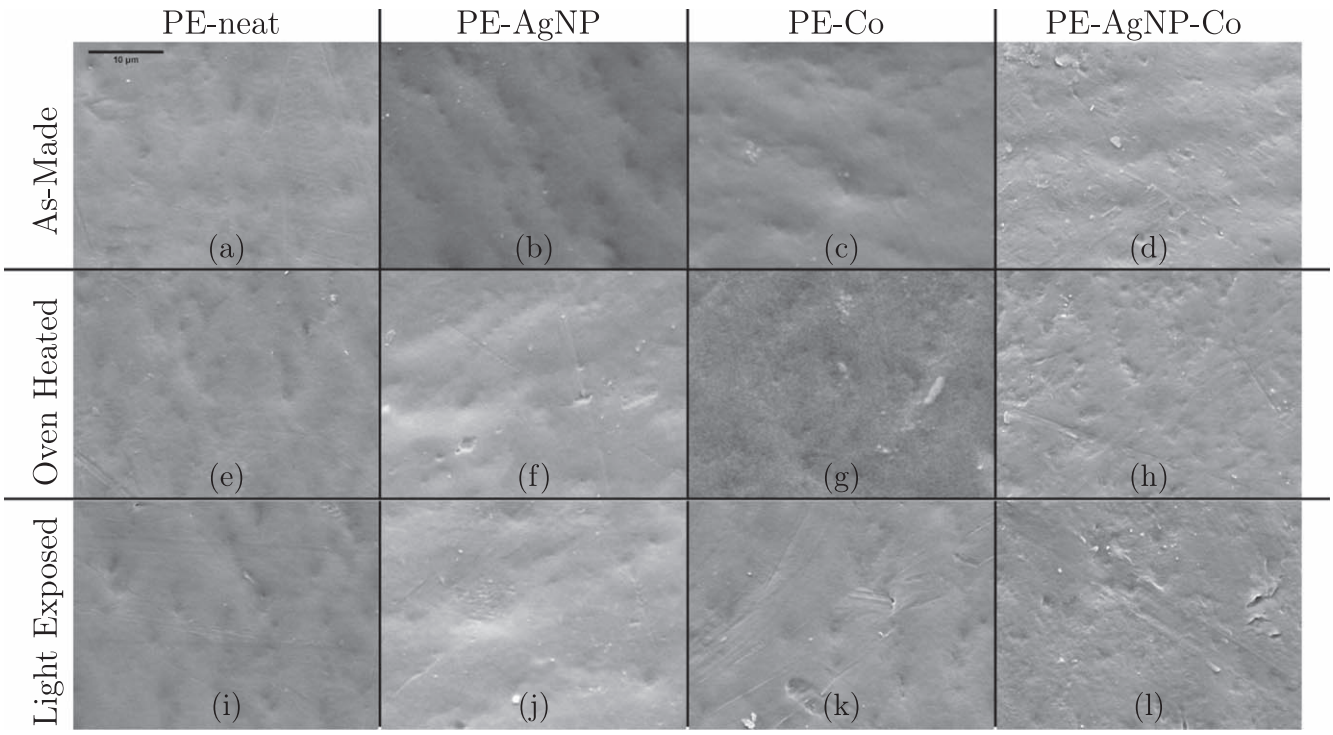

Figure 9. 30 μm by 40 μm SEM images of LDPE film surfaces as made (a)–(d), and after exposure to conventional heating (e)–(h) or under illumination (i)–(l) for 120 h.

significant enhancement in degradation products as a function of light exposure. As previously mentioned, such samples rapidly warm to an average temperature of approximately 55 °C (see section 2.7). In fact, comparing the photothermally-heated PE-AgNP-Co case (blue triangles), in which heat is generated from application of visible light, to the conventionally-heated case (blue-squares), in which heat is applied through convective mechanisms in the dark to similar average temperature, shows that the results are almost identical. This indicates that the average sample temperature is the driving factor for carbonyl creation, rather than the peak sample temperature. The peak sample temperature (which is located near each nanoparticle under photothermal heating) is expected to significantly exceed the average temperature due to the low concentration of AgNP in the samples, with large interparticle spacing (1 μm) and moderate light intensity [4, 41, 43, 45]. The strong similarity of the data is also consistent with the hypothesis that for this chemical reaction scheme the heterogeneity of the temperature field present in photothermal heating is neither a detriment nor an advantage. These measurements also indicate that reactions taking place due to heating from ambient light and a sensitizer would result in the same chemical by-products as an 'accelerated aging' laboratory experiment utilizing a conventionally-heated sample and that, autonomous accelerated aging in the environment might be possible. We note that PE-Co samples (without AgNPs, red triangles) degraded very slightly as a function of light exposure, likely due to the small increased ambient temperature within the LED illumination area (i.e. 36 °C ± 2 °C). The difference between the response of the PE-AgNP-Co samples (blue triangles) and the PE-Co samples (red triangles), shows the effect of the AgNPs as a sensitizing agent, significantly increasing the absorption of light and enabling energy 'harvest' from the visible light source.

3.3. Comparison of mechanical properties as a function of heating modality

As discussed in the introduction, changes in mechanical properties have important practical consequences when considering polymer degradation. The heterogeneous temperature distribution present during photothermal heating could in principle generate mechanical defects, and thereby likely enhance micro-fragmentation. In the next two sub-sections, the bulk mechanical properties and micromorphology (via electron microscopy) of LDPE is examined to determine if such deleterious effects are intensified under photothermal heating. Figure 8 summarizes the mechanical properties of LDPE formulations before and after exposure to conventional heat or light (which may or may not heat depending on the presence of AgNP). The neat LDPE sample as-made was found to have modulus at 1% strain of 197 ± 22 MPa, stress at break of 11.7 ± 1.8 MPa, and strain at break of 628 ± 103%, consistent with the manufacturers specifications for this material. Incorporation of additives showed no significant changes in any of these properties prior to aging (i.e. comparing the as-made (red bars) for different formulations). In general, early-stage oxidative degradation in LPDE most strongly affects strain at break (elongation) [71]. Low molecular weight regions where chain scission has occurred represent mechanical defects. Elongating the sample exposes a significant volume to stress and breakage occurs when a

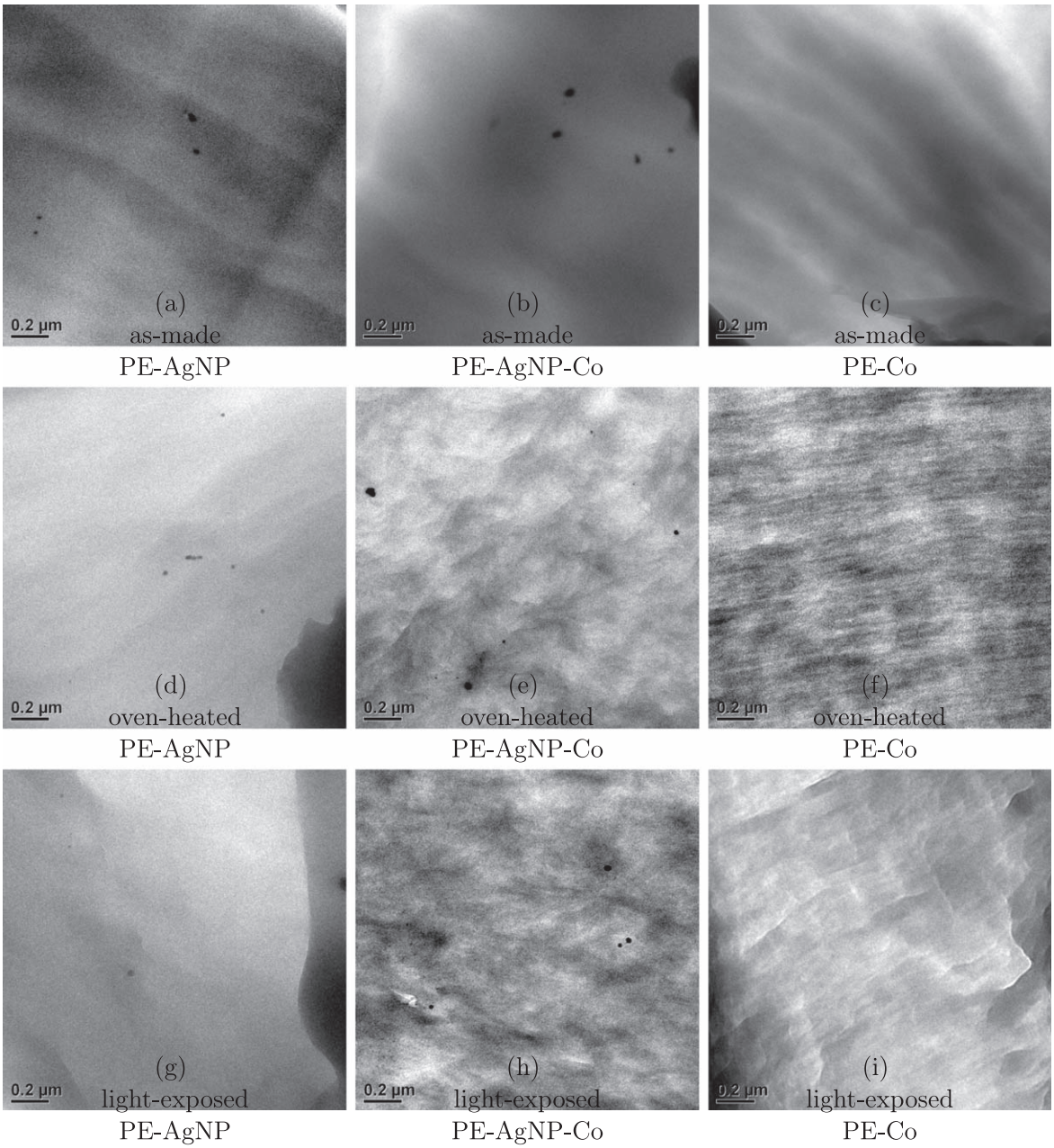

Figure 10. 1.8 μm by 1.8 μm cross-sectional TEM micrographs of LDPE samples as-made (a)–(c), and after accelerated aging via conventional heating (d)–(f) or light exposure (h)–(i). Images were intentionally captured near the copper grid (black areas in the images) to provide contrast.

defect enhances the local stress to beyond a critical value. Thus, defects prevent significant elongation because the sample breaks and can also lower the observed stress at break. In contrast, modulus value reflects only the initial response to deformation, and thus, is robust to defect formation.

First we consider the innate changes in mechanical properties due to the thermo-oxidative degradation via conventional means. After 120 h in a 55 °C–60 °C oven (red bars), cobalt-free samples (PE-neat, first column, and PE-AgNP, second column) showed no significant change from as-made samples (green bars) in any measured property, which is consistent with the observation (via spectroscopy) of no chemical changes within these formulations. Again, at these time scales, only cobalt-catalyzed oxidation is observable. Samples containing cobalt (PE-Co, third column, and PE-AgNP-Co, fourth column) displayed catastrophic loss of maximum strain (top row), breaking at 21 ± 4.5% and 22 ± 3%, respectively, less than one-twentyfifth of the as-made value. As expected [72], modulus and stress at break showed weaker effects, modulus was slightly increased (252 ± 10 MPa and 247 ± 8 MPa, respectively) and stress at break decreased slightly (10.8 ± 0.3 MPa and 10.7 ± 0.3 MPa, respectively).

For illuminated samples, after aging for 120 h under 0.27 W cm^{-2} blue light (blue bars), neither cobalt-free sample (PE-neat, first column, and PE-AgNP, second column) showed significant change in any tested property compared to

as-made samples. As discussed in the previous section, samples being illuminated experienced a slightly elevated ambient temperature of 36 °C, which resulted in small changes to PE-Co samples (third column, blue bar) including a minor reduction in strain at break. Overall these results confirm that the LED light source does not produce sufficient UV light to damage polyethylene via photo-oxidation and that thermo-oxidation is the dominant process under these conditions.

In contrast to the small effect from the waste heat produced by the light source (PE-Co, see above), samples that contained both cobalt and light-to-heat converting AgNPs (PE-AgNP-Co, fourth column, comparing the green and blue bars) displayed significant changes in mechanical properties as a function of light exposure. In particular, a catastrophic loss of strain at break from 535 ± 101% to 10 ± 4% and a decrease in stress at break to 9.2 ± 1.1 MPa was observed. As with the carbonyl measure, changes in mechanical properties were very similar to oven-treated specimens that experienced the same average temperature. Polymer fracture is governed by defects, making tensile testing very sensitive to defect creation. However, no difference was observed between the conventional and photothermal methods, indicating that the photothermal process did not produce significantly more defects than the conventional treatment.

These observations are consistent with the hypothesis that the distributed nature of the oxidative reaction, requiring oxygen (more abundant near the sample outer edges), cobalt (randomly distributed throughout the sample), and heat from the AgNPs, means that the reactions in the immediate vicinity of the hot nanoparticles are not a significant fraction of the chemistry occurring within the sample. Rather, the AgNPs primarily serve as an energy conduit with a large cross-section (i.e. likely larger than their physical area [73]) which collects light and then highly efficiently [4, 74] converts this optical energy into internal heat that then diffuses to a reaction site.

3.4. Surface and internal morphology from electron microscopy

Examining internal and surface sample morphology also enables assessment of defect formation. Figure 9 summarizes SEM studies of the surface morphology of LDPE formulations before and after conventional heating or light exposure for 120 h. The as-made PE-neat (figure 9(a)) displays a complex surface including sub-10 μm dimpling as well as larger linear features and a slight surface roughness. It is likely these features are most representative of the constrained conditions of the surface at the time of melt pressing. The addition of either AgNPs or cobalt stearate (figures 9(b), (c)) has no noticeable effect on the surface morphology of as-made samples, whereas both in combination show increased striation and more specks, which do not change with aging. Surface damage (such as cracking and pitting where a portion of material at the surface has been removed) are common under photo-oxidation with UV light of PE containing pro-degradant additives [75–78]. No increase in such features was observed in the samples exposed to visible light in this study (figures 9(i)–(l)).

A useful approach is to compare the surface morphology of samples of the particular type that have experienced thermo-oxidative degradation to those that have not. All as-made samples (figures 9(a)–(d)) and samples without Co present (images e, f, i, j) displayed no evidence of oxidation in both spectroscopic and mechanical studies. Notice the range of morphology observed in these cases, which includes roughness, puckering, and linear marks. One can compare these cases to those where significant thermo-oxidative degradation was observed via spectroscopic and mechanical means (figures 9(g), (h), (l)). No trend in surface morphology is present. Thermo-oxidated samples resulting from conventional heating (figures 9(g), (h)) had identical morphology to those produced via photothermal activity (figure 9(l)). Thus surface imaging studies show no evidence of additional defect formation (or heterogeneous processing) due to the photothermal process.

Changes in internal morphology were investigated via TEM images of micro-tomed cross-sectional slices of LDPE samples as-made (figures 10(a)–(c)) and after (figures 10(d)–(i)) exposure to accelerated aging conditions. Note that the dispersion of AgNPs in unaged samples is discussed in section 2.2. Samples containing AgNPs (figures 10(d), (e), (g), (h)) showed no change to the AgNPs morphology, confirming the stability of the nanoparticles under mild heating or photothermal excitation, even in the presence of pro-oxidant cobalt ions. Alterations to the LDPE matrix are difficult to interpret conclusively using traditional TEM techniques. It is again useful to compare samples of the same type with and without thermo-oxidation. Unaged samples (figures 10(a)–(c)) and samples without Co (images d, g) have an evidently smoother (or more uniform) appearance than those in which thermo-oxidation has occurred (images e, f, h). These textural changes may represent differences in the fracture dynamics of the aged LDPE during microtoming. We note the light-exposed PE-Co samples (image i), which only experience very slight thermo-oxidation (and a maximum temperature of 36 °C), also have a textured appearance.

TEM studies might also show evidence of inhomogeneous degradation in the immediate vicinity of the AgNPs which experiences much higher temperatures than the sample average. However, the LDPE matrix showed no localized damage surrounding AgNP that could be attributed to such an effect in samples that were heated photothermally. In particular, comparing PE-AgNP-Co degraded with conventional heating (image e) to those via a photothermal approach (image h), the regions around the nanoparticles are comparable. Thus, TEM studies provide additional support to the inference that most of the chemical reactions occur relatively far from each AgNP, mitigating the effect of the heterogeneous temperature field within the sample.

4. Conclusion

We demonstrate that the addition of a dilute photothermal sensitizer enables control of degradation processes in LDPE using light. Due to plasmonic silver nanoparticles' high photothermal conversion efficiency, extremely low loading (less than 0.1 wt%) was able to produce sufficient temperatures to aid degradation, thus minimizing any effect of their addition on the LDPE physical properties. A method for incorporation of AgNPs into LDPE with minimal solvent use was developed and shown to have no noticeable effect on the mechanical properties of the resulting nanocomposite. When exposed to intense, resonant light, heat from the nanoparticles accelerated the action of the thermal pro-oxidant cobalt stearate on LDPE to a rate equal to placing samples into a 60 °C oven. The degradation process was evaluated by FTIR and UV–vis absorption spectroscopy, which revealed that the photothermally-driven process evolved residual products (carbonyl containing species) in the same proportion and at the same rate as conventionally-driven thermal degradation. The heterogeneity of the photothermally-driven process was evaluated by electron microscopy and examining mechanical properties. In the vicinity of the nanoheaters where temperatures were highest, the polymer matrix showed no additional degradation. No preferential deterioration was observed at the surfaces of films either, since light is selectively absorbed by the additives distributed throughout the matrix and not by the polymer itself. This lack of heterogeneity implies that the risk of fragmentation of films is not significantly increased by the photothermal degradation modality.

Acknowledgments

This work was supported by the National Science Foundation (CMMI-1462966). We would like to thank the Analytical Services Laboratory (NCSU Textile Engineering, Chemistry, and Science), Dr Keith Weninger (NCSU Physics), and the Education and Research Laboratory (NCSU physics) for use of equipment. The authors thank Dr Carrie J Thomas (NCSU MEAS) and Dr Russell E Gorga (NCSU TECS) for helpful discussions. We acknowledge NCSU Physics department support of the senior design program, as well as Matt Mims, Tamar McMahon, Daniela Fontecha, Chad Barrow, Ashleigh Cuomo, and Erik Lutz for aid in constructing the blue light degradation apparatus. This work was performed in part at the Analytical Instrumentation Facility (AIF), which is supported by the State of North Carolina and the National Science Foundation (Award Number ECCS-1542015). The AIF is a member of the North Carolina Research Triangle Nanotechnology Network (RTNN), a site in the National Nanotechnology Coordinated Infrastructure (NNCI).

ORCID iDs

Gabriel Firestone https://orcid.org/0000-0001-6139-0522
Jason R Bochinski https://orcid.org/0000-0002-2643-5737
Laura I Clarke https://orcid.org/0000-0003-1863-571X

References

[1] Neumann O, Urban A S, Day J, Lal S, Nordlander P and Halas N J 2013 Solar vapor generation enabled by nanoparticles *ACS Nano* **7** 42–9
[2] Siregar S, Oktamuliani S, Saijo Y and Theoretical A 2018 Model of laser heating carbon nanotubes *Nanomaterials* **8** 580
[3] Loeb S, Li C and Kim J-H 2018 Solar photothermal disinfection using broadband-light absorbing gold nanoparticles and carbon black *Environ. Sci. Technol.* **52** 205–13
[4] Govorov A O and Richardson H H 2007 Generating heat with metal nanoparticles *Nano Today* **2** 30–8
[5] Lal S, Clare S E and Halas N J 2008 Nanoshell-enabled photothermal cancer therapy: impending clinical impact *Acc. Chem. Res.* **41** 1842–51
[6] Qin Z and Bischof J C 2012 Thermophysical and biological responses of gold nanoparticle laser heating *Chem. Soc. Rev.* **41** 1191–217
[7] Maity S, Downen L N, Bochinski J R and Clarke L I 2011 Embedded metal nanoparticles as localized heat sources: an alternative processing approach for complex polymeric materials *Polymer* **52** 1674–85
[8] Viswanath V, Maity S, Bochinski J R, Clarke L I and Gorga R E 2013 Thermal annealing of polymer nanocomposites via photothermal heating: effects on crystallinity and spherulite morphology *Macromolecules* **46** 8596–607
[9] Viswanath V, Maity S, Bochinski J R, Clarke L I and Gorga R E 2016 Enhanced crystallinity of polymer nanofibers without loss of nanofibrous morphology via heterogeneous photothermal annealing *Macromolecules* **49** 9484–92
[10] Mintenig S, Int-Veen I, Löder M, Primpke S and Gerdts G 2017 Identification of microplastic in effluents of waste water treatment plants using focal plane array-based micro-Fourier-transform infrared imaging *Water Res.* **108** 365–72
[11] Depledge M, Galgani F, Panti C, Caliani I, Casini S and Fossi M 2013 Plastic litter in the sea *Mar. Environ. Res.* **92** 279–81
[12] Jambeck J R, Geyer R, Wilcox C, Siegler T R, Perryman M, Andrady A, Narayan R and Law K L 2015 Plastic waste inputs from land into the ocean *Science* **347** 768–71
[13] Koelmans A A, Gouin T, Thompson R, Wallace N and Arthur C 2014 Plastics in the marine environment *Environ. Toxicol. Chem.* **33** 5–10
[14] Hermabessiere L, Dehaut A, Paul-Pont I, Lacroix C, Jezequel R, Soudant P and Duflos G 2017 Occurrence and effects of plastic additives on marine environments and organisms: a review *Chemosphere* **182** 781–93
[15] Gregory M R 2009 Environmental implications of plastic debris in marine settingsentanglement, ingestion, smothering, hangers-on, hitch-hiking and alien invasions *Phil. Trans. R. Soc.* B **364** 2013–25
[16] Besseling E, Wegner A, Foekema E M, van den Heuvel-Greve M J and Koelmans A A 2013 Effects of microplastic on fitness and PCB bioaccumulation by the lugworm arenicola marina (L.) *Environ. Sci. Technol.* **47** 593–600
[17] Moore C J 2008 Synthetic polymers in the marine environment: a rapidly increasing, long-term threat *Environ. Res.* **108** 131–9
[18] Westphalen H and Abdelrasoul A 2018 *Water Challenges of an Urbanizing World* (Rijeka: InTech)
[19] Sun J, Dai X, Wang Q, van Loosdrecht M C and Ni B-J 2019 Microplastics in wastewater treatment plants: detection, occurrence and removal *Water Res.* **152** 21–37

[20] O'Donovan S, Mestre N C, Abel S, Fonseca T G, Carteny C C, Cormier B, Keiter S H and Bebianno M J 2018 Ecotoxicological effects of chemical contaminants adsorbed to microplastics in the clam scrobicularia plana *Frontiers Mar. Sci.* **5** 143

[21] Diepens N J and Koelmans A A 2018 Accumulation of plastic debris and associated contaminants in aquatic food webs *Environ. Sci. Technol.* **52** 8510–20

[22] Kwon J-H, Chang S, Hong S H and Shim W J 2017 Microplastics as a vector of hydrophobic contaminants: Importance of hydrophobic additives *Integr. Environ. Assess. Manage.* **13** 494–9

[23] Koelmans A A, Bakir A, Burton G A and Janssen C R 2016 Microplastic as a vector for chemicals in the aquatic environment: critical review and model-supported reinterpretation of empirical studies *Environ. Sci. Technol.* **50** 3315–26

[24] Pilař J, Michálková D, Šlouf M, Vacková T and Dybal J 2014 Heterogeneity of accelerated photooxidation in commodity polymers stabilized by HAS: ESRI, IR, and MH study *Polym. Degrad. Stab.* **103** 11–25

[25] Gardette M, Perthue A, Gardette J L, Janecska T, Földes E, Pukánszky B and Therias S 2013 Photo- and thermal-oxidation of polyethylene: comparison of mechanisms and influence of unsaturation content *Polym. Degrad. Stab.* **98** 2383–90

[26] Colin X, Audouin L, Verdu J, Rozental-Evesque M, Rabaud B, Martin F and Bourgine F 2009 Aging of polyethylene pipes transporting drinking water disinfected by chlorine dioxide. Part II-Lifetime prediction *Polym. Eng. Sci.* **49** 1642–52

[27] Thomas R T, Nair V and Sandhyarani N 2013 TiO_2 nanoparticle assisted solid phase photocatalytic degradation of polythene film: a mechanistic investigation *Colloids Surf.* A **422** 1–9

[28] Yang R, Christensen P A, Egerton T A, White J R and Maltby A 2011 Spectroscopic studies of photodegradation of polyethylene films containing TiO_2 nanoparticles *J. Appl. Polym. Sci.* **119** 1330–8

[29] Zenteno A, Lieberwirth I, Catalina F, Corrales T, Guerrero S, Vasco D A and Zapata P A 2017 Study of the effect of the incorporation of TiO_2 nanotubes on the mechanical and photodegradation properties of polyethylenes *Composites* B **112** 66–73

[30] Zapata P A, Rabagliati F M, Lieberwirth I, Catalina F and Corrales T 2014 Study of the photodegradation of nanocomposites containing TiO_2 nanoparticles dispersed in polyethylene and in poly(ethylene-co-octadecene) *Polym. Degrad. Stab.* **109** 106–14

[31] Kamalian P, Khorasani S N, Abdolmaleki A and Neisiany R E 2019 Grafted ZnO nanoparticles used for development in photocatalytic degradation performance of polyethylene *Polym. Bull.* **76** 3593–606

[32] Gryn'ova G, Hodgson J L and Coote M L 2011 Revising the mechanism of polymer autooxidation *Org. Biomol. Chem.* **9** 480–90

[33] Thompson R C 2004 Lost at sea: where is all the plastic? *Science* **304** 838–838

[34] Kalogerakis N, Karkanorachaki K, Kalogerakis G C, Triantafyllidi E I, Gotsis A D, Partsinevelos P and Fava F 2017 Microplastics generation: onset of fragmentation of polyethylene films in marine environment mesocosms *Frontiers Mar. Sci.* **4** 84

[35] Weinstein J E, Crocker B K and Gray A D 2016 From macroplastic to microplastic: degradation of high-density polyethylene, polypropylene, and polystyrene in a salt marsh habitat *Environ. Toxicol. Chem.* **35** 1632–40

[36] Wegner A, Besseling E, Foekema E, Kamermans P and Koelmans A 2012 Effects of nanopolystyrene on the feeding behavior of the blue mussel (Mytilus edulis L.) *Environ. Toxicol. Chem.* **31** 2490–7

[37] Gouin T, Roche N, Lohmann R and Hodges G 2011 A thermodynamic approach for assessing the environmental exposure of chemicals absorbed to microplastic *Environ. Sci. Technol.* **45** 1466–72

[38] Hidalgo-Ruz V and Thiel M 2013 Distribution and abundance of small plastic debris on beaches in the SE Pacific (Chile): a study supported by a citizen science project *Mar. Environ. Res.* **87–88** 12–8

[39] Jain P K, Lee K S, El-Sayed I H and El-Sayed M A 2006 Calculated absorption and scattering properties of gold nanoparticles of different size, shape, and composition: applications in biological imaging and biomedicine *J. Phys. Chem.* B **110** 7238–48

[40] Arnold M D and Blaber M G 2009 Optical performance and metallic absorption in nanoplasmonic systems *Opt. Express* **17** 3835

[41] Hogan N J, Urban A S, Ayala-Orozco C, Pimpinelli A, Nordlander P and Halas N J 2014 Nanoparticles heat through light localization *Nano Lett.* **14** 4640–5

[42] Mackey M A, Ali M R K, Austin L A, Near R D and El-Sayed M A 2014 The most effective gold nanorod size for plasmonic photothermal therapy: theory and *in vitro* experiments *J. Phys. Chem.* B **118** 1319–26

[43] Maity S, Wu W C, Xu C, Tracy J B, Gundogdu K, Bochinski J R and Clarke L I 2014 Spatial temperature mapping within polymer nanocomposites undergoing ultrafast photothermal heating via gold nanorods *Nanoscale* **6** 15236–47

[44] Ma H, Bendix P M and Oddershede L B 2012 Large-scale orientation dependent heating from a single irradiated gold nanorod *Nano Lett.* **12** 3954–60

[45] Maity S, Wu W-C, Tracy J B, Clarke L I and Bochinski J R 2017 Nanoscale steady-state temperature gradients within polymer nanocomposites undergoing continuous-wave photothermal heating from gold nanorods *Nanoscale* **9** 11605–18

[46] Gomes L B, Klein J M, Brandalise R N, Zeni M, Zoppas B C and Grisa A M C 2014 Study of oxo-biodegradable polyethylene degradation in simulated soil *Mater. Res.* **17** 121–6

[47] Bonhomme S, Cuer A, Delort A-M, Lemaire J, Sancelme M and Scott G 2003 Environmental biodegradation of polyethylene *Polym. Degrad. Stab.* **81** 441–52

[48] Portillo F, Yashchuk O and Hermida L 2016 Evaluation of the rate of abiotic and biotic degradation of oxo-degradable polyethylene *Polym. Test.* **53** 58–69

[49] Lee B H, Cho J W and Kim K H 2017 Crystallization, orientation, and mechanical properties of laser-heated photothermally drawn polypropylene/multi-walled carbon nanotube fibers *Eur. Polym. J.* **91** 70–80

[50] Song X, Wang Y, Wang C, Huang M, Gul S and Jiang H 2019 Solar-intensified ultrafiltration system based on porous photothermal membrane for efficient water treatment *ACS Sustain. Chem. Eng.* **7** 4889–96

[51] Tosini G, Ferguson I and Tsubota K 2016 Effects of blue light on the circadian system and eye physiology *Mol. Vis.* **22** 61–72

[52] Arsenault H, Hébert M and Dubois M-C 2012 Effects of glazing colour type on perception of daylight quality, arousal, and switch-on patterns of electric light in office rooms *Build. Environ.* **56** 223–31

[53] Albertsson A-C, Andersson S O and Karlsson S 1987 The mechanism of biodegradation of polyethylene *Polym. Degrad. Stab.* **18** 73–87

[54] Skibida I P 1975 Kinetics and mechanism of the decomposition of organic hydroperoxides in the presence of transition metal compounds *Russ. Chem. Rev.* **44** 789–800

[55] Prasad B L, Arumugam S K, Bala T and Sastry M 2005 Solvent-adaptable silver nanoparticles *Langmuir* **21** 822–6
[56] Bulavchenko A I, Arymbaeva A T, Demidova M G, Popovetskiy P S, Plyusnin P E and Bulavchenko O A 2018 Synthesis and concentration of organosols of silver nanoparticles stabilized by AOT: emulsion versus microemulsion *Langmuir* **34** 2815–22
[57] Taleb A, Petit C and Pileni M P 1997 Synthesis of highly monodisperse silver nanoparticles from AOT reverse micelles: a way to 2D and 3D self-organization *Chem. Mater.* **9** 950–9
[58] Singha D, Barman N and Sahu K 2014 A facile synthesis of high optical quality silver nanoparticles by ascorbic acid reduction in reverse micelles at room temperature *J. Colloid Interface Sci.* **413** 37–42
[59] Paramelle D, Sadovoy A, Gorelik S, Free P, Hobley J and Fernig D G 2014 A rapid method to estimate the concentration of citrate capped silver nanoparticles from UV–visible light spectra *Analyst* **139** 4855–61
[60] Dolinnyi A I 2017 Extinction coefficients of gold nanoparticles and their dimers. Dependence of optical factor on particle size *Colloid J.* **79** 611–20
[61] Polemi A and Shuford K L 2012 Distance dependent quenching effect in nanoparticle dimers *J. Chem. Phys.* **136** 184703
[62] Lakshmana Rao J, Narendra G and Lakshman S 1990 Optical absorption spectra of cobalt(II) and nickel(II) ions in lead acetate glasses *Polyhedron* **9** 1475–7
[63] Brode W R 1928 The Analysis of the Absorption Spectrum of Cobalt Chloride in Concentrated Hydrochloric Acid *Proc. R. Soc.* A **118** 286–95
[64] Maity S, Bochinski J R and Clarke L I 2012 Metal nanoparticles acting as light-activated heating elements within composite materials *Adv. Funct. Mater.* **22** 5259–70
[65] Maity S, Kozek K A, Wu W C, Tracy J B, Bochinski J R and Clarke L I 2013 Anisotropic thermal processing of polymer nanocomposites via the photothermal effect of gold nanorods *Part. Part. Syst. Charact.* **30** 193–202
[66] Abbott D B, Maity S, Burkey M T, Gorga R E, Bochinski J R and Clarke L I 2014 Blending with non-responsive polymers to incorporate nanoparticles into shape-memory materials and enable photothermal heating: the effects of heterogeneous temperature distribution *Macromol. Chem. Phys.* **215** 2345–56
[67] Dong J, Firestone G E, Bochinski J R, Clarke L I and Gorga R E 2017 *In situ* curing of liquid epoxy via gold-nanoparticle mediated photothermal heating *Nanotechnology* **28** 1–9
[68] Firestone G, Bochinski J R, Meth J S and Clarke L I 2018 Facile measurement of surface heat loss from polymer thin films via fluorescence thermometry *J. Polym. Sci.* B **56** 643–52
[69] Kuzma A *et al* 2012 Influence of surface oxidation on plasmon resonance in monolayer of gold and silver nanoparticles *J. Appl. Phys.* **112** 103531
[70] Sheldon R A and Kochi J K 1981 *Metal-Catalyzed Oxidations of Organic Compounds* (Amsterdam: Elsevier) pp 33–70
[71] Fayolle B, Colin X, Audouin L and Verdu J 2007 Mechanism of degradation induced embrittlement in polyethylene *Polym. Degrad. Stab.* **92** 231–8
[72] Hsu Y C, Weir M P, Truss R W, Garvey C J, Nicholson T M and Halley P J 2012 A fundamental study on photo-oxidative degradation of linear low density polyethylene films at embrittlement *Polymer* **53** 2385–93
[73] Bohren C F and Huffman D R 2007 *Absorption and Scattering of Light by Small Particles* (Weinheim, Germany: Wiley-VCH Verlag GmbH) pp 475–6
[74] Eustis S and El-Sayed M A 2006 Why gold nanoparticles are more precious than pretty gold: noble metal surface plasmon resonance and its enhancement of the radiative and nonradiative properties of nanocrystals of different shapes *Chem. Soc. Rev.* **35** 209–17
[75] Vidya F, Raghul S S, Bhat S G and Thachil E T 2011 Effect of cobalt stearate and vegetable oil on UV and biodegradation of linear lowdensity poly(ethylene)-poly(vinyl Alcohol) blends *Polym. Renew. Resour.* **2** 131–48
[76] Ali S S, Qazi I A, Arshad M, Khan Z, Voice T C and Mehmood C T 2016 Photocatalytic degradation of low density polyethylene (LDPE) films using titania nanotubes *Environ. Nanotechnol., Monit. Manage.* **5** 44–53
[77] Stark N M 2003 Photodegradation and photostabilization of weathered wood flour filled polyethylene composites *PhD Thesis* Michigan Technological University
[78] Suresh B, Maruthamuthu S, Kannan M and Chandramohan A 2011 Mechanical and surface properties of low-density polyethylene film modified by photo-oxidation *Polym. J.* **43** 398–406